
Revealing the learning process in reinforcement learning agents through attention-oriented metrics

Charlotte Beylier

Max Planck Institute for Human Cognitive and Brain Sciences
Center for Scalable Data Analytics and Artificial Intelligence (ScaDS.AI)
Dresden/Leipzig, Germany
beylier@cbs.mpg.de

Simon M. Hofmann

Max Planck Institute for Human Cognitive and Brain Sciences
Leipzig, Germany
simon.hofmann@cbs.mpg.de

Nico Scherf

Max Planck Institute for Human Cognitive and Brain Sciences
Center for Scalable Data Analytics and Artificial Intelligence (ScaDS.AI)
Dresden/Leipzig, Germany
nscherf@cbs.mpg.de

Abstract

The learning process of a reinforcement learning (RL) agent remains poorly understood beyond the mathematical formulation of its learning algorithm. To address this gap, we introduce attention-oriented metrics (ATOMs) to investigate the development of an RL agent’s attention during training. We tested ATOMs on three variations of a Pong game, each designed to teach the agent distinct behaviours, complemented by a behavioural assessment. Our findings reveal that ATOMs successfully delineate the attention patterns of an agent trained on each game variation, and that these differences in attention patterns translate into differences in the agent’s behaviour. Through continuous monitoring of ATOMs during training, we observed that the agent’s attention developed in phases, and that these phases were consistent across games. Finally, we noted that the agent’s attention to its paddle emerged relatively late in the training and coincided with a marked increase in its performance score. Overall, we believe that ATOMs could significantly enhance our understanding of RL agents’ learning processes, which is essential for improving their reliability and efficiency.

1 Introduction

Understanding the learning process of a deep Reinforcement Learning (RL) agent is critical for improving its transparency and performance. However, the mechanisms unfolding during an agent’s learning phase remain largely unknown beyond the mathematical formulations of its algorithm and optimisation process. Therefore, new metrics are needed to provide insights into what an RL agent learns about its environment and its task during training.

Currently, the primary indicator of an agent’s learning progress is its performance score derived from task-specific rewards. While necessary to optimize an agent Watkins and Dayan [1992],

Konda and Tsitsiklis [1999], Mnih et al. [2013], this performance score provides a very limited view of an agent’s development during learning and fails to explain or predict certain behaviours in the testing phase. For instance, RL agents have been observed exploiting faulty reward functions Clark and Amodei [2016] while achieving high performance scores during training, or showing significant divergence during the test phase despite similar training performances Cobbe et al. [2019]. These examples underscore the limitations of this metric in fully understanding an agent’s behaviours and development.

In this context, explainable AI (XAI) methods can complement the limitation of the performance score by providing an insight into an agent understanding of its environment and task through the explanation of its decisions Verma et al. [2018], Shu et al. [2017]. However, the explanation format given by these methods - which may be a decision tree Liu et al. [2019], a structural causal model Madumal et al. [2020] or a set of linguistic rules Hein et al. [2017] - is often too complex to be tracked during learning. Methods focused on saliency maps on the other hand, are easier to compute and are more versatile but are mostly used in a qualitative way to explain the behaviour of trained agent Zeiler and Fergus [2014], Zhou et al. [2016], Weitekamp et al. [2018], Selvaraju et al. [2017]. As a results XAI techniques do not give information during the learning phase of an agent.

In this work we introduce attention-oriented metrics (ATOMs) to gain insight into an agent’s learning process through the development of its attention. ATOMs is derived from saliency maps and combine the traceability of the performance score metric with the explanatory power of XAI and quantify an agent’s attention on the objects within its environment. Specifically, ATOMs encompass two levels of description:

- the ranked attention on individual objects (*hierarchical-attention*), and
- the attention on combinations of such objects (*combinatorial-attention*).

To systematically evaluate ATOMs’ ability to give information about what an RL agent has learned, we created three variation of a Pong game. Each variation required the agent to learn distinct behaviour. In addition to these games, we designed a behavioural experiment to test if the agent’s attention described by ATOMs translated into their observed behaviour Atrey et al. [2019].

Our main contributions are:

- We introduce ATOMs that quantify an agent’s attention to objects in its environment, using *Hierarchical-attention* and *Combinatorial-attention* metrics.
- We present three variation of the Pong game, each designed to induce distinct behaviour in agents.
- We show that ATOMs can provide insights into what an agent has learned about its game and that successfully trained agents developed similar, game-specific, attention patterns.
- We used ATOMs to follow the development of an agent’s attention during its training and identified distinct phases of attention patterns common to all agents in our experiments. Additionally, we found that the agent’s self-attention developed late in the learning and coincided with a significant increase in its performance score.

2 Related work

Explainable RL Explainable RL methods have been developed to elucidate the decision-making process in RL agents. Some methods aim to enhance the interpretability of the policy an agent has learned. This is achieved by encoding the policy in a human-understandable form, such as a decision tree Liu et al. [2019], Coppens et al. [2019], Roth et al. [2019], a set of linguistic rules Hein et al. [2017] or a domain specific (programming) language Verma et al. [2018]. Other methods decompose a complex policy into several simpler ones such as in Shu et al. [2017] where the general policy is decomposed into local policies corresponding to elementary skills that have been manually annotated by humans. The global, more complex policy is then employed to determine which local policy to apply along the agent’s trajectory. Alternative techniques propose a justification for the model actions using structural causal models Madumal et al. [2020] or a justification for the general policy with a language understandable by humans Hayes and Shah [2017], van der Waa et al. [2018]. Last but not least, a number of methods rely on visual explanations of an agent’s behaviour. These

include projection methods Zahavy et al. [2016] that use the agent’s neural population activity to display the pattern learned by its network. Whilst previous studies on saliency maps tend to focus on fully trained models, we propose using them to study the learning dynamics that occur during model training.

Saliency maps Saliency maps have widely been used to explain predictions of deep image classifiers in computer vision, but have been increasingly used as an exploratory tool for RL models Zeiler and Fergus [2014], Zhou et al. [2016], Weitkamp et al. [2018], Selvaraju et al. [2017]. There are two main types of saliency maps: gradient based Greydanus et al. [2018] and perturbation-based Puri et al. [2019] methods. Gradient-based methods estimate the significance of each input pixel on the network’s decision-making process by analyzing the gradient with respect to these pixels. In contrast, perturbation-based methods estimate this influence by individually altering each pixel and observing the resultant effect on the network’s choice of action. Nonetheless, perturbation-based methods necessitate multiple forward passes for each input, which rend them significantly computationally expensive Xing et al. [2023]. Gradient-based methods are faster, but are also subject to noise. We chose Layer-wise Relevance Propagation (LRP) Bach et al. [2015], Lapuschkin et al. [2019], as it can be computed efficiently, while overcoming the noise problem many gradient methods share.

3 Methods

3.1 Experimental setup

Data were recorded in actor-critic agents (A2C; Konda and Tsitsiklis [1999]) from the Stable Baseline 3 repository Raffin et al. [2021]. We study the actor network of each agent, responsible for the choice of action. This network is composed of three convolutional layers (size 4x32, 32x64 64x64) followed by a linear layer (size 1x512) that we will refer to as F_c (Fig 1 a) and a final output layer. Throughout the remainder of this paper, we will use the terms ‘agent’ and ‘actor network’ synonymously. The agent’s strategy was derived from the activity of neurons in the linear layer (F_c). This layer is located just before the output layer and encompasses the final *world-model* on which the agent choose its action. ATOMs are computed from this layer.

3.2 Attention-Oriented Metrics (ATOMs)

ATOMs are composed of two metrics evaluating different aspects of an agent’s attention: the *hierarchical-attention* and the *combinatorial-attention* metrics. The hierarchical-attention evaluates the degree of attention given to an individual object compared to the other objects. In contrast, the combinatorial-attention evaluates how much attention an agent pays simultaneously to different combinations of objects. This simultaneous attention could be an indicator of a latent variable encoded by the neuron. Here we characterize the Pong game by its constituent objects: the paddles of the agent and its opponent, their respective displayed score, both balls ($B1$ and $B2$) and the walls. Figure 1 a illustrates the process to extract these two metrics.

Both metrics composing ATOMs are derived from the attention of the neurons in the F_c layer that are relevant to an action. Specifically, this attention is measured by computing Layer-Wise Relevance Propagation (LRP; Bach et al. [2015], Lapuschkin et al. [2019]). For a model output $f(\mathbf{x})$ (here at the action node), LRP calculates a relevance score for each neuron in the previous layer. Due to its conservation property, relevance can be propagated layer-by-layer up until the input (here images) resulting in a relevance map per layer. To generate input images \mathbf{x} (consisting of pixels p) used for the LRP analysis, we let an agent play the game for ten episodes. Subsequently, we filtered the input to ensure all objects are present and have a spacing of 10 pixels between them to prevent overlap. We then sampled a total of 200 frames and automatically labeled the objects within each frame. Let $\mathbf{X} \in \mathbb{R}^{200 \times 4 \times 84 \times 84}$ and $\bar{\mathbf{X}} \in \mathbb{R}^{200 \times 4 \times 84 \times 84}$ be the original and the labeled version of the input set, respectively. We focus on the attention of neurons influencing action choices, identifying relevant neurons in the F_c layer using LRP.

For each input, $\mathbf{x} \in \mathbf{X}$:

1. Calculate the relevance scores $R_{F_c} = \{R_i\}_{i \in F_c}$ and select neurons $S \subseteq F_c$ that account for 90% of the total relevance R_{F_c} . This filtering step is used to avoid noise components and decrease ATOMs computational time.

2. Generate relevance maps at the model input $\mathbf{R}^k(\mathbf{x}) = \{R_p^k(\mathbf{x})\}$ for each neuron $k \in S$
3. Identify the objects highlighted by the relevance maps.

Hierarchical-attention We first characterize an agent’s attention by identifying which objects are most important to the network’s decision-making. We do this by using a hierarchical-attention metric $h : O \rightarrow \mathbb{R}$, to measure the importance of each object. For objects $o_g \in O$, the hierarchical-attention metric h and its components are defined as follows:

$$h(o_g) = \frac{1}{|\mathbf{X}|} \sum_{\mathbf{x} \in \mathbf{X}} \sum_{k \in S} R_k(\mathbf{x}) \cdot \bar{R}_g^k(\mathbf{x}), \quad (1)$$

$$\bar{R}_g^k(\mathbf{x}) = \frac{1}{V} \sum_{p \in P_{o_g}} R_p^k(\mathbf{x}), \quad \text{where } V = |R_{p_g}^k(\mathbf{x}) \setminus \{0\}|, \quad (2)$$

and p_g denotes all pixels $p \in o_g$.

Combinatorial-attention We then incorporate the combinations of objects that an agent simultaneously attends to by using the combinatorial-attention metric $c : O \rightarrow \mathbb{R}$. For a subset of objects $T \subseteq O$, the combinatorial-attention metric is defined as follows:

$$c(T) = \frac{1}{|\mathbf{X}|} \sum_{\mathbf{x} \in \mathbf{X}} \sum_{k \in S} R_k(\mathbf{x}) \cdot \delta_k(\mathbf{x}; T), \quad (3)$$

$$\delta_k(\mathbf{x}; T) = \begin{cases} 1 & \text{if } \bar{R}_g^k(\mathbf{x}) > \beta \text{ for all } g \in T \text{ and } \bar{R}_g^k(\mathbf{x}) = 0 \text{ for all } g \in O \setminus T, \\ 0 & \text{else.} \end{cases} \quad (4)$$

where $\beta = \alpha \cdot M^k$ with $\alpha = 0.25$ and $M^k = \max_g(\{\bar{R}_g^k(\mathbf{x})\}_g)$.

An illustration of different combination of objects looked at by neurons in the F_c layer can be found in appendix D (figure 1). The impact of the α threshold on the results of the combinatorial-attention metric is discussed in appendix E.

3.3 Measurements of ATOMs during training

The frequency of evaluation (f_r), denoting how often the metrics were extracted, was chosen for each game based on the training dynamics observed. We set $f_r = 230$ for version v_0 , $f_r = 85$ for version v_1 and $f_r = 50$ for version v_2 . The choice of f_r for each game was influenced by the number of epochs required for the network to demonstrate an increase in training score in the respective game. It’s important to note that different frequencies could be selected based on the desired granularity for studying the evolution of the metrics. Our selected frequencies aimed to balance the need for detailed metric tracking with the practical constraints of computational resources and training time.

3.4 Designing Pong variations

We implemented three different variations of the Pong game: $v0$, $v1$, and $v2$. Each variant builds on the classic Pong gameplay where two agents compete with each other, each controlling a paddle to score points by returning the ball to the opponent’s side. A point is awarded when the ball passes the opponent’s paddle and an episode terminate when a player accumulates 21 points. For training, a reward of +1 or -1 is assigned depending on which side scores. $v0$ maintains traditional gameplay. In $v1$, two balls are present ($B1$ and $B2$), but only $B1$ counts for scoring while $B2$ is used as a distraction. In $v2$, both $B1$ and $B2$ are integral, but $B2$ only interacts with the agent’s paddle, awarding +1 for a rebound and -1 if it passes the paddle. Additionally, in $v2$, the agent must reach 41 points, while the opponent needs only 21 to win. Figure 1b illustrates the three game variations. Details regarding the game implementation and the rules can be found in Appendix C.

3.5 Evaluating agent behaviour: Dual Ball Discrimination Test

A major difference between the three game variations is the importance of ball $B1$ and ball $B2$. As the latter only yield rewards in $v2$ we expect the behaviour of the agents toward $B2$ to change between

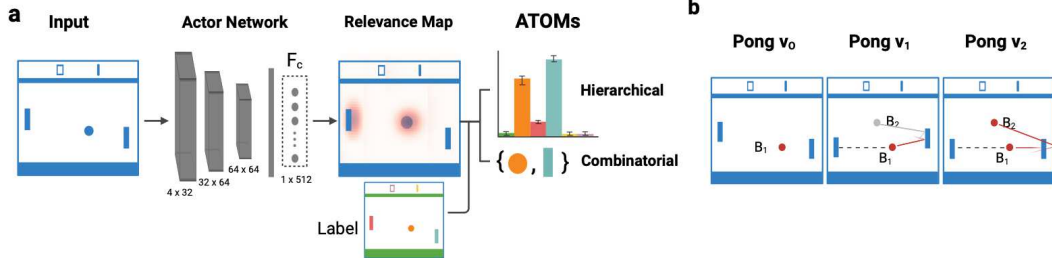


Figure 1: **a** ATOMs consists of two metrics (hierarchical, and combinatorial attention) that summarize the agent’s attention. These metrics are derived from relevance maps generated using the LRP method, applied to a typical game state, where all objects are simultaneously presented. **b** Illustration of the three variations of the Pong game. Red balls yield reward to the agent. In v_1 the gray ball is a distractor. The balls’ dynamics are illustrated with lines indicating if a ball bounces back from the opponent or passes through it.

games. To quantitatively evaluate agent behaviour, we implemented the *Dual Ball Discrimination Test*, wherein the agent is put in a situation enforcing a choice between both balls. This experiment involved generating 100 unique trajectories from various initial positions and velocities, designed such that both balls reach the agent’s x-coordinate simultaneously while maintaining a separation exceeding the length of the paddle. Consequently, the agent can interact with only one of the balls and we can analyse any systematic preference for B_1 or B_2 . An illustration of the test is displayed figure 3 a.

4 Experiments

4.1 Evaluation of ATOMs

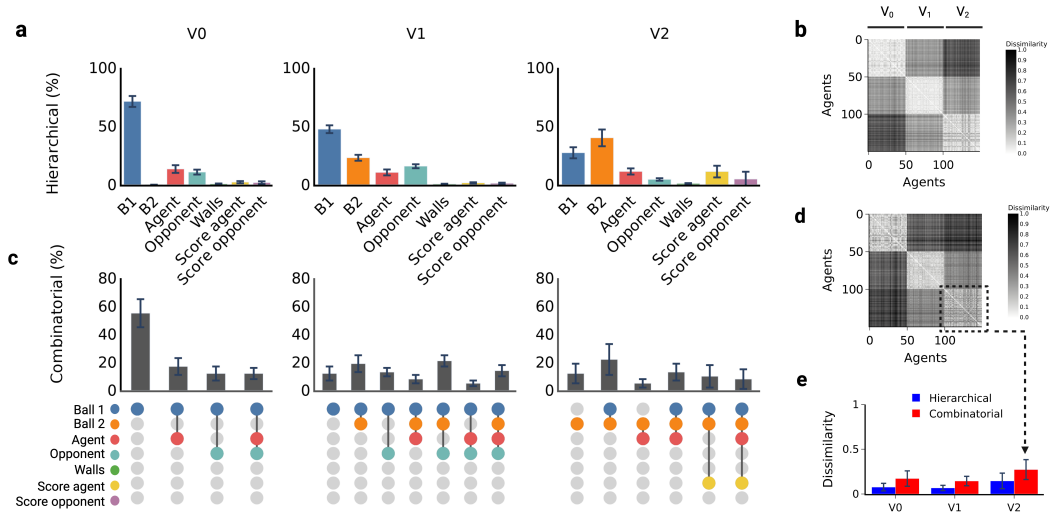


Figure 2: **a** Hierarchical profile averaged over 50 trained agents for each game variation. **b** Dissimilarity matrix for the hierarchy-attention metrics for all agents. **c** Combinatorial-attention metric which examines co-observation of objects by individual neurons. Each object is symbolized by a distinct coloured dot. Combinations of objects are indicated through the simultaneous colouring of two or more dots. **d** Dissimilarity matrix for the combinatorial-attention metrics for all agents. **e** Dissimilarity between agents within game variation for the hierarchy and the combinatorial-attention metrics. Error bars represent standard-deviation values.

We evaluated the capacity of ATOMs to provide relevant information about what an agent has learned. To this end, we computed ATOMs on 50 fully trained agents for each game variation: v_0 ,

$v1$, $v2$. Agents were trained using different random initialization (details regarding agent training protocols are provided in B).

Different game variations induce game-specific attention pattern. The hierarchical-attention (figure 2 a) shows that trained agents attended to the expected aspects of the game. Notably, agents trained on $v0$ and $v1$ paid more attention to ball $B1$ (the only ball that brings a reward) while agents trained on $v2$ (in which both balls yield rewards) showed a more nuanced attention pattern with a slight preference for the ball $B2$. Across all game variations, the second highest attention was consistently directed towards the agent and opponent paddles. Interestingly, agents from $v2$ developed attention to the score displayed on the game screen as well.

The combinatorial-attention (figure 2 c) further breaks down the attention of the neurons in the F_c layer into combination of objects. We found a consistent common pattern across game variations with attention to either the ball(s) alone or to a combination of ball(s) and the agent’s paddle or ball(s) and the opponent’s paddle. Figures 2 b,d show that successfully trained agent developed similar attention patterns as the similarity in both ATOMs metrics are higher within game variation. Interestingly, we observed greater variability in the combinatorial-attention metrics (figure 2 e) in variation $v2$ compared to $v1$ and $v0$ indicating that agents may develop more diverse attention patterns in game variations that are more complex.

Attention patterns are consistent with agents’ behaviour. As shown in figure 2 a, ATOMs indicate that agents trained on $v1$ still paid attention to $B2$ suggesting that these agents had not learned to ignore the ball completely. To investigate this further, we examined whether the attention directed towards $B1$ and $B2$ reflected the agent’s behaviour, which we defined here as the relative interaction of the agent with each of the balls. Specifically, we assessed whether increased attention to one ball over the other reflected a preference for interacting with that particular ball. To study this experimentally, we exposed agents trained on game variation $v1$ or $v2$ to the *Dual Ball Discrimination Test* 3.5 to measure how often the agent interacted with each ball (figure 3 a). Figure 3 b shows the proportion of $B1$ interactions relative to $B2$ interactions against the importance given to $B1$ relative to $B2$. Distinct clusters emerge that correspond to variations $v1$ and $v2$. This shows that the relative attention given to each ball indeed reflects how an agent behaves towards them (in terms of preferred interaction). Furthermore, the cluster associated with $v1$ shows that these agents still interact with $B2$, confirming the hypothesis driven by the ATOMs metrics that agents in $v1$ had not learned to ignore $B1$ completely.

As mentioned, agents trained on $v2$ developed an attention to the score displayed on the screen (figure 2 a). This prompted us to analyse the impact of the displayed score on the agent’s behaviour. While this may be an artifact of an increased spatial attention in the more complex game variant, the results of the *Dual Ball Discrimination Test* reveal that the displayed scores indeed influenced the agent’s choice to hit $B1$ or $B2$. Distinct patterns of influence were observed among agents. For instance, some agents exhibited a preference for $B1$ until their displayed score approached 40 points, at which point they tended to choose $B2$ (the game terminates when the agent reaches 41 points). Other agents shifted their preference from $B1$ to $B2$ once the displayed score of the opponent exceeded 10 points. Further details of the experiments and results are provided in Appendix F.

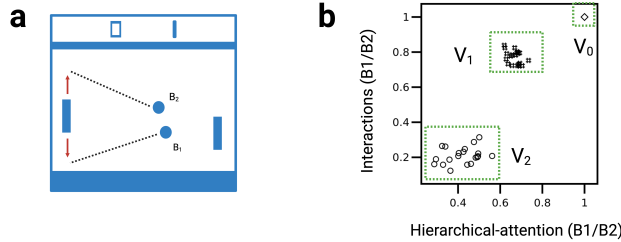


Figure 3: **a** Dual Ball Discrimination Test, 100 trajectories were generated such that the agent is forced to choose between interacting with $B1$ or $B2$. **b** Relative interaction of $B1$ with respect to $B2$ in function of the relative hierarchy of $B1$ with respect to $B2$. $v0$ was added as a reference.

4.2 Evolution of agents' attention during learning

We then monitored the development of the agents' attention during their training using ATOMs.

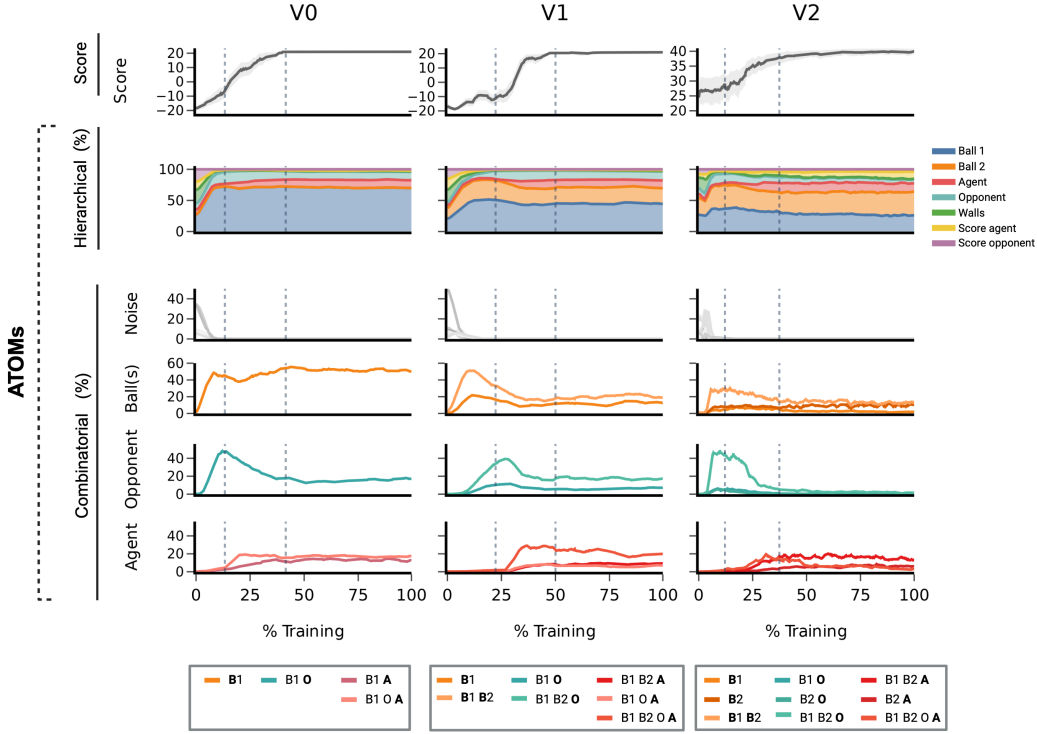


Figure 4: Development of the performance score and ATOMs during learning for each game version. The performance scores of the agent were computed for ten games at each point of measurement during training. The average score is depicted by the central dark line, with the shaded region representing \pm the standard deviation. The dotted lines indicate the time frame during which the agent's score showed a marked increase. These time frames were picked manually. The combinatorial-attention is categorized as follows from top to bottom: noise (grey), combinations of balls only (orange), combinations of opponent and balls (cyan), and combinations of objects including the agent itself (red)

Application of ATOMs during training Figure 4 illustrates ATOMs for three agents trained on $v0$, $v1$ and $v2$ alongside their performance during training. The results reveals that most pronounced changes in the hierarchical metric occurred at the initial stage of the training preceding a marked enhancement in the agent's performance. While the hierarchical metric indicates the overall importance of an object, the combinatorial metrics dissect this information further by revealing to which combination of objects an agent pays attention to. In this figure, we categorized the plots of the combinatorial metrics into four major groups:

- combinations involving only $B1$ and $B2$ (Ball(s)),
- combinations involving the balls and the opponent (Opponent),
- combinations involving the agent (Agent),
- combinations of objects only present during the initial learning phase (Noise).

The evolution of the combinatorial-attention during training shows how the attention of an agent gets progressively selective to specific subsets of objects. For example, by looking at the evolution of the attention to the ball(s) for the games $v1$ and $v2$, one can see that the agent's attention started by including both ball objects ($B1$, $B2$). Then as the training progress its attention progressively isolated the individual balls ($B1$ in $v1$ and $B1$ and $B2$ in $v2$).

Attention patterns develop in phases during learning The four categories defined above appeared to follow a timeline consistent amongst versions $v0$, $v1$ and $v2$ (Figure 4). We will therefore refer to these categories as phases. In the first phase the attention was non-selective and spread among objects (Noise phase). In the following phase the agents focused most attention upon the moving ball(s). Subsequently, the agents also paid attention to the opponent. Finally, in the "Agent phase", agents paid attention to themselves in relation to the other objects. Interestingly, this phase was consistently the last one to emerge and coincide with a marked increase in the agents' performance scores (indicated by the two dotted lines in figure 5) ¹. To test if these phases were consistent among all agents, we repeated this analysis with ten agents per version and measured their phase onsets (figure 5). We defined the onset of a phase as the point at which the first component composing this phase exceeds 25% of its maximum value. This onset was then expressed as a percentage of the total training period for a given agent, with the total training period being the time taken for an agent to reach its maximum score. We found that the timeline of these attention phases were consistent across models and game versions.

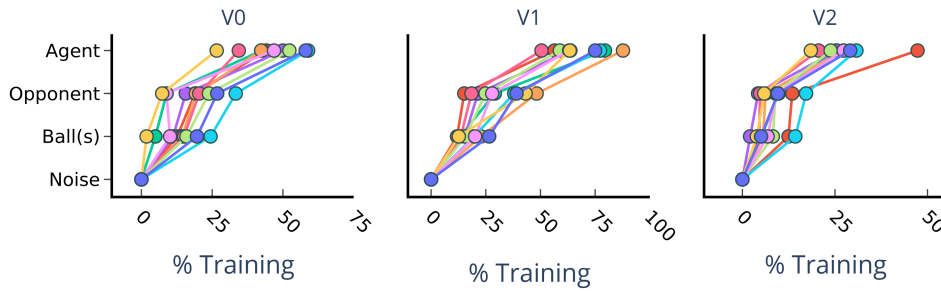


Figure 5: Onset of the attention phases (Noise, Ball(s), Opponent, Agent) for each agent (represented by different colours) in game versions $\text{textit{v0}}$, $\text{textit{v1}}$, and $\text{textit{v2}}$. Each phase is composed of one or several components . The onset of a phase is defined as the point at which the first component composing this phase exceeds 25% of its maximum value. This onset is then expressed as a percentage of the total training period for a given agent.

5 Discussion

The learning process of an RL agent is poorly understood beyond the mathematical equations of its learning algorithm. In this study we delve deeper into the learning phase of an agent by analyzing the development of its attention. To this end, we introduce Attention-Oriented Metrics (ATOMs) designed to quantitatively assess an agent's attention. We evaluated ATOMs' ability to give information about what an RL agent has learned, by implementing three versions of a Pong game, each requiring the agent to learn distinct behaviour.

Our results demonstrated that ATOMs successfully delineate the different attention patterns that each game version induces. More specifically, we observed that successfully trained agents exhibited consistent, game-specific attention patterns. Additionally, behavioural tests revealed that these divergent attention patterns corresponded to observable differences in agent behaviour. Through continuous monitoring of ATOMs during training, we identified distinct, sequentially ordered developmental phases in its attention. Notably, an agent's attention to itself emerged relatively late in the learning process coinciding with an increase in its performance score. We suggest that an agent's attention is guided by the association of objects' movements - or more generally changes in the state of an object- with reward feedback. Indeed, in our three games, the most straightforward correlation between an object's movement and a feedback reward involves the movement of the ball(s), either by passing the agent side or the opponent's side, or by hitting the agent's paddle (for $B2$ in version $v2$). Since the opponent is designed to score points, its movement is correlated with future rewards as well. Conversely, as the agent learns to play pong its actions are less likely to influence the feed-

¹Agents trained on game $v2$ developed an additional attention component that integrated the scores of the agent and/or of the opponent (results in appendix 6)

back reward. This difference could explain the agent’s initial focus on the ball(s) and the opponent and the late focus to the paddle it controls.

While ATOMs offer valuable insights about RL agent development during learning, they have limitations that could be addressed in future work. Indeed, ATOMs are object-based, which, while reflecting our human understanding of the games, may limit their explanatory power. Alternative metrics based on an agent’s attention, not limited to the object level, could reveal more subtle abstractions or reasoning underlying an agents’ decision-making processes. Additionally, ATOMs requires image labeling and are best suited to environments with a limited set of objects, as its combinatorial-attention component grows polynomially with the number of objects potentially diminishing its explanatory power.

Despite these constraints, we believe that ATOMs can enhance our understanding of the learning process of RL agents, and offer several potential applications. For instance, monitoring an agent’s attention could ensure its focus on the pertinent objects (either during training or online) particularly in safety-critical applications. It could also facilitate the early detection of flawed policies or exploitation of bugs in an environment which might not be evident through performance scores alone. For example, in our experiments, agents trained on *v1* had not learn to fully ignore the irrelevant ball despite achieving an optimal performance score. This suggest potential refinement in the environment design or in the reward function. Thus, accessing an agent’ attention during its training could accelerate the debugging of the environments and reward functions.

Acknowledgments

N.S., C.B. and S.H. are supported by BMBF (Federal Ministry of Education and Research) through ACONITE (01IS22065) and the Center for Scalable Data Analytics and Artificial Intelligence (ScaDS.AI.) Dresden/Leipzig. C.B. is also supported by the Max Planck IMPRS NeuroCom Doctoral Program. The figures were created using BioRender.com.

References

- Christopher JCH Watkins and Peter Dayan. Q-learning. *Machine learning*, 8:279–292, 1992.
- Vijay Konda and John Tsitsiklis. Actor-critic algorithms. *Advances in neural information processing systems*, 12, 1999.
- Volodymyr Mnih, Koray Kavukcuoglu, David Silver, Alex Graves, Ioannis Antonoglou, Daan Wierstra, and Martin Riedmiller. Playing atari with deep reinforcement learning. *arXiv preprint arXiv:1312.5602*, 2013.
- Jack Clark and Dario Amodei. Faulty reward functions in the wild. *Internet: <https://blog.openai.com/faulty-reward-functions>*, 2016.
- Karl Cobbe, Oleg Klimov, Chris Hesse, Taehoon Kim, and John Schulman. Quantifying generalization in reinforcement learning. In *International Conference on Machine Learning*, pages 1282–1289. PMLR, 2019.
- Abhinav Verma, Vijayaraghavan Murali, Rishabh Singh, Pushmeet Kohli, and Swarat Chaudhuri. Programmatically interpretable reinforcement learning. In *International Conference on Machine Learning*, pages 5045–5054. PMLR, 2018.
- Tianmin Shu, Caiming Xiong, and Richard Socher. Hierarchical and interpretable skill acquisition in multi-task reinforcement learning. *arXiv preprint arXiv:1712.07294*, 2017.
- Guiliang Liu, Oliver Schulte, Wang Zhu, and Qingcan Li. Toward interpretable deep reinforcement learning with linear model u-trees. In *Machine Learning and Knowledge Discovery in Databases: European Conference, ECML PKDD 2018, Dublin, Ireland, September 10–14, 2018, Proceedings, Part II 18*, pages 414–429. Springer, 2019.
- Prashan Madumal, Tim Miller, Liz Sonenberg, and Frank Vetere. Explainable reinforcement learning through a causal lens. In *Proceedings of the AAAI conference on artificial intelligence*, volume 34, pages 2493–2500, 2020.
- Daniel Hein, Alexander Hentschel, Thomas Runkler, and Steffen Udfluft. Particle swarm optimization for generating interpretable fuzzy reinforcement learning policies. *Engineering Applications of Artificial Intelligence*, 65:87–98, 2017.

- Matthew D Zeiler and Rob Fergus. Visualizing and understanding convolutional networks. In *European conference on computer vision*, pages 818–833. Springer, 2014.
- Bolei Zhou, Aditya Khosla, Agata Lapedriza, Aude Oliva, and Antonio Torralba. Learning deep features for discriminative localization. In *Proceedings of the IEEE conference on computer vision and pattern recognition*, pages 2921–2929, 2016.
- Laurens Weitekamp, Elise van der Pol, and Zeynep Akata. Visual rationalizations in deep reinforcement learning for atari games. In *Benelux Conference on Artificial Intelligence*, pages 151–165. Springer, 2018.
- Ramprasaath R Selvaraju, Michael Cogswell, Abhishek Das, Ramakrishna Vedantam, Devi Parikh, and Dhruv Batra. Grad-cam: Visual explanations from deep networks via gradient-based localization. In *Proceedings of the IEEE international conference on computer vision*, pages 618–626, 2017.
- Akanksha Atrey, Kaleigh Clary, and David Jensen. Exploratory not explanatory: Counterfactual analysis of saliency maps for deep reinforcement learning. *arXiv preprint arXiv:1912.05743*, 2019.
- Youri Coppens, Kyriakos Efthymiadis, Tom Lenaerts, Ann Nowé, Tim Miller, Rosina Weber, and Daniele Magazzeni. Distilling deep reinforcement learning policies in soft decision trees. In *Proceedings of the IJCAI 2019 workshop on explainable artificial intelligence*, pages 1–6, 2019.
- Aaron M Roth, Nicholay Topin, Pooyan Jamshidi, and Manuela Veloso. Conservative q-improvement: Reinforcement learning for an interpretable decision-tree policy. *arXiv preprint arXiv:1907.01180*, 2019.
- Bradley Hayes and Julie A Shah. Improving robot controller transparency through autonomous policy explanation. In *Proceedings of the 2017 ACM/IEEE international conference on human-robot interaction*, pages 303–312, 2017.
- Jasper van der Waa, Jurriaan van Diggelen, Karel van den Bosch, and Mark Neerinx. Contrastive explanations for reinforcement learning in terms of expected consequences. *arXiv preprint arXiv:1807.08706*, 2018.
- Tom Zahavy, Nir Ben-Zrihem, and Shie Mannor. Graying the black box: Understanding dqns. In *International conference on machine learning*, pages 1899–1908. PMLR, 2016.
- Samuel Greydanus, Anurag Koul, Jonathan Dodge, and Alan Fern. Visualizing and understanding atari agents. In *International conference on machine learning*, pages 1792–1801. PMLR, 2018.
- Nikaash Puri, Sukriti Verma, Piyush Gupta, Dhruv Kayastha, Shripad Deshmukh, Balaji Krishnamurthy, and Sameer Singh. Explain your move: Understanding agent actions using specific and relevant feature attribution. *arXiv preprint arXiv:1912.12191*, 2019.
- Jinwei Xing, Takashi Nagata, Xinyun Zou, Emre Neftci, and Jeffrey L Krichmar. Achieving efficient interpretability of reinforcement learning via policy distillation and selective input gradient regularization. *Neural Networks*, 161:228–241, 2023.
- Sebastian Bach, Alexander Binder, Grégoire Montavon, Frederick Klauschen, Klaus-Robert Müller, and Wojciech Samek. On pixel-wise explanations for non-linear classifier decisions by layer-wise relevance propagation. *PloS one*, 10(7):e0130140, 2015.
- Sebastian Lapuschkin, Stephan Wäldchen, Alexander Binder, Grégoire Montavon, Wojciech Samek, and Klaus-Robert Müller. Unmasking clever hans predictors and assessing what machines really learn. *Nature communications*, 10(1):1096, 2019.
- Antonin Raffin, Ashley Hill, Adam Gleave, Anssi Kanervisto, Maximilian Ernestus, and Noah Dormann. Stable-baselines3: Reliable reinforcement learning implementations. *Journal of Machine Learning Research*, 22(268):1–8, 2021. URL <http://jmlr.org/papers/v22/20-1364.html>.

A LRP relevance score derivation

Let $f : \mathbb{R}^n \rightarrow \mathbb{R}^m$ be the feedforward neural network characterizing an agent's network policy, where, $\mathbf{x} \in \mathbb{R}^n$ is the input image to the network, and $f(\mathbf{x}) \in \mathbb{R}^m$ is its output. The function f representing the neural network can be defined as $f(\mathbf{x}) = f_L \circ f_{L-1} \circ \dots \circ f_1(\mathbf{x})$ with each $f_{l \in L}$ representing a transformation at layer l .

Applied to an input image \mathbf{x} , LRP Bach et al. [2015], Lapuschkin et al. [2019] calculates a relevance score $R_p(\mathbf{x})$ for each pixel $p \in \mathbf{x}$, indicating the pixel's importance in the network's decision. The output of the LRP method is a relevance map or heatmap, represented as $\mathbf{R}(\mathbf{x}) = \{R_p(\mathbf{x})\}_{p \in \mathbf{x}}$. $\mathbf{R}(\mathbf{x})$ is derived by iteratively backpropagating the network output $f(\mathbf{x})$ from layer $l+1$ to layer l according to some backpropagation rules. These backpropagation rules are guided by a relevance model as detailed by Montavon et al. [2017] which can be expressed in their general form by:

$$R_{i \in l} = \sum_{j \in l+1} \frac{q_{ij}}{\sum_{i' \in l} q_{i'j}} R_j \quad (1)$$

where R_i is the relevance of the neuron $i \in l$ and R_j is the relevance of the neuron $j \in l+1$. Here, q_{ij} varies depending on the chosen relevance propagation rule, which is contingent on the input domain of the data Montavon et al. [2017]. In our experiments, the data consist of either pixel values p or outputs from a ReLU activation function, both of which are positive real number. Consequently, we employ the z^+ -rule for backpropagation. Within this framework, $q_{ij} = x_i w_{ij}^+$, where x_i represents the activity output of neuron i , and w_{ij}^+ is the positive part of the weight connecting neurons i and j .

Common procedure In our research, we want to determine the extent to which specific regions of an input image \mathbf{x} contribute to the activation of a particular neuron in the F_c layer. Given input \mathbf{x} , we consider where a neuron is looking at in the input. To do so we apply the following steps for each input, $\mathbf{x} \in \mathbf{X}$:

1. Calculate the distributed relevance scores $R_{F_c} = \{R_i\}_{i \in F_c}$. Identify and select the subset of neurons $S \subseteq F_c$ that collectively account for 90% of the total relevance R_{F_c} .
2. For each neuron $k \in S$, generate the corresponding relevance map in the input space denoted $\mathbf{R}^k(\mathbf{x}) = \{R_p^k(\mathbf{x})\}$.
3. Identify the objects highlighted by the relevance maps.

1. Calculate the distributed relevance scores $\{R_i\}_{i \in F_c}$

To compute $\{R_i\}_{i \in F_c}$ we backpropagate the output relevance $\mathbf{R}_{\text{output}}$ back to the neurons in the F_c layer using the propagation formula applied with the z^+ -rule. We initialize $\mathbf{R}_{\text{output}} = f(\mathbf{x})$ and then following equation (1):

$$R_{i \in F_c} = \sum_{j \in f(\mathbf{x})} \frac{x_i w_{ij}^+}{\sum_{i' \in F_c} x_{i'} w_{i'j}^+} \cdot j \quad (2)$$

We then order the neurons by their relevance score and select the smallest subset S responsible for at least 90% of the total relevance score.

2. For each neuron $k \in S$ generate $\mathbf{R}^k(\mathbf{x}) = \{R_p^k(\mathbf{x})\}_{p \in \mathbf{x}}$

Here $R^k(\mathbf{x})$ is the relevance of neuron k in layer F_c with regard to the network's output $f(\mathbf{x})$. $R_p^k(\mathbf{x})$ is the relevance of pixel $p \in \mathbf{x}$ with regard to the neuron k output.

To compute $\{R^k(\mathbf{x})\}_{k \in S}$ we backpropagate the relevance score of neuron k to the input space. In this step, we are only interested in *where* the neuron k is looking on the input image and not its relative contribution to the choice of the action. We therefore initialize the new relevance distribution at the F_c layer by setting $R_{F_c} = (t_1, \dots, t_k, \dots, t_N)$ where $t_i = 0$ for all $i \neq k$ and $t_k = 1$ where k is the index of the neuron under study. The relevance R_{F_c} is then backpropagated through the layers of the network until the input \mathbf{x} using the backpropagation formula in (1), such that,

$$R_i = \sum_j \frac{x_i w_{ij}^+}{\sum_{i'} x_{i'} w_{i'j}^+} R_j \quad (3)$$

This results in a relevance map over the input \mathbf{x} which in combination with the corresponding labeled input $\bar{\mathbf{x}}$ allow us to retrieve where the input the network is looking. We used Fischer [2021] for the implementation of the LRP method.

B RL training procedure

For all games the learning rate was set to $\alpha = 7e - 4$, the discount factor $\gamma = 0.99$, the entropy coefficient $\tau = 0.01$ and the value loss coefficient $v_{lc} = 0.25$. The number of parallel environment was set to $n = 100$. Training was conducted on Nvidia via A100 GPUs using a single GPU with up to 18 CPU cores per task and a memory of 125 GB.

C Game

C.1 Game Dynamics Setup

We developed a modified version of the classic Atari Pong game using the Pygame library (v.2.5.2 Shinnars [2011]) to create a custom environment for our experiments. This variation maintains the original game’s elements—paddles, walls, and scoring—but introduces dual balls instead of one. The dimensions and colors of the game components mirror those in the original Pong. In this setup, each paddle is distinctively colored, as are the two balls. Paddles moves on the y-axis at a rate of 2 pixels per frame, while the balls move at speeds of 4 pixels per frame along the x-axis and 2 pixels per frame on the y-axis. Game states are represented as 84x84 pixel RGB images.

C.2 Preprocessing and Environment Wrapping

To prepare the game environment for reinforcement learning (RL), we encapsulated it within the same preprocessing wrapper used for Atari games in the Stable Baselines 3 framework (v.3 Raffin et al. [2021]). This wrapper converts each game frame from RGB to grayscale to streamline input dimensions and reduce computational demands Mnih et al. [2013]. To prevent the RL agent from memorizing action sequences, we introduced randomness in the initial ball direction. Last but not the least, the observation input given to the agent is not Markovian as all the information necessary to predict the next input given this input and an action is not available. Aligning with prior research by Y and common practices in Stable Baselines 3, we stacked four consecutive frames, producing a composite input $o_t \in R^{4 \times 84 \times 84}$, to provide the agent with a temporal context for decision-making.

C.3 Variations

Game variations are summarized in the Table Y.

Table 1: Design of the game variations

	Ball 1	Ball 2	B1 D	B2 D	B1 R	B2 R
V0	Yes	No	D1	x	R1	x
V1	Yes	Yes	D1	D1	R1	x
V2	Yes	Yes	D1	D2	R1	R2

Dynamics:

- D1: The ball rebounds off both the walls and the paddles.
- D2: The ball is capable of bouncing off the walls and the agent’s paddle. However, it will not rebound off the opponent’s paddle, and pass through it.

Rewards:

- R1: The agent is awarded +1 for scoring a point on the opponent’s side, and receives a -1 if the agent fails to hit the ball, allowing it to pass by.

- R2: The agent gains +1 for successfully hitting the ball with their paddle. Conversely, a -1 penalty is applied if the agent fails to hit the ball, allowing it to pass by.

The balls start on the middle of the screen. They have the same x-direction which is randomly generated and opposite y-directions. This choice of Initial states forces the agent to choose between the balls for the first hit. The condition for an episode to end and for the balls to respawn is dependent on *BI* being scored. The opponent is hard-coded to position its y-axis on the y-axis of *BI*.

D Example combinatorial-attention

Figure 1 presents various combinatorial-attention patterns for individual neurons in the F_c layer. Each neuron’s relevance map, generated for a specific input, is overlaid onto the input provided to the agent. The right side features a bar plot quantifying the average intensity of relevance scores for each object, with a dotted line indicating the 25% threshold of the maximum intensity value.

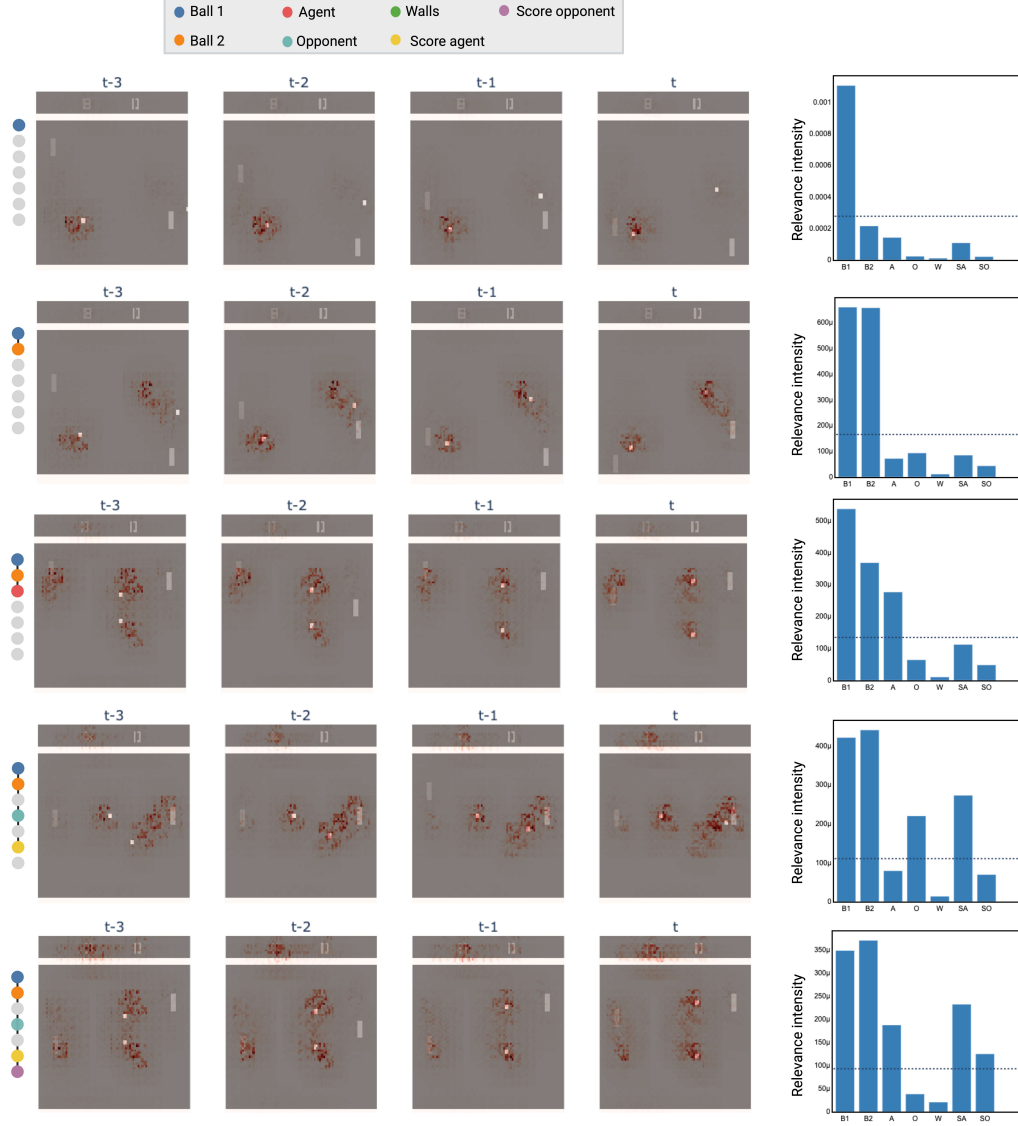


Figure 1: Illustrations of different combinatorial-attention results. Each line represents a combination of objects "looked at" by a neuron in the F_c layer. From left to right: symbol of the combination as depicted in the main text, neuron’s relevance map overlaid onto the input frames, bar plot quantifying the average intensity of relevance scores for each object with the 25% threshold.

E Threshold value for the combinatorial-attention

The threshold value, α , utilized in the combinatorial-attention metric functions as a hyperparameter and influences the metric's outcome. It sets the minimum intensity level necessary for an object to be considered within the set of observed objects. A threshold approaching zero will result in a combinatorial-attention metric that accounts for all objects with any non-zero intensity score. Conversely, a threshold near one will reflect combinatorial-attention equivalent to only the single object with the highest intensity value. To avoid these extremes, we choose a threshold of $\alpha = 0.25$. This value allows for the detection of more nuanced patterns of combinatorial attention. To demonstrate the dependency of the combinatorial-attention metric on the threshold value, calculations were conducted across a range of threshold values from 0 to 1 for all 20 trained agents in each version of the game. Figure 2 illustrates the average combinatorial-attention metric across models as a function of α for each game version.

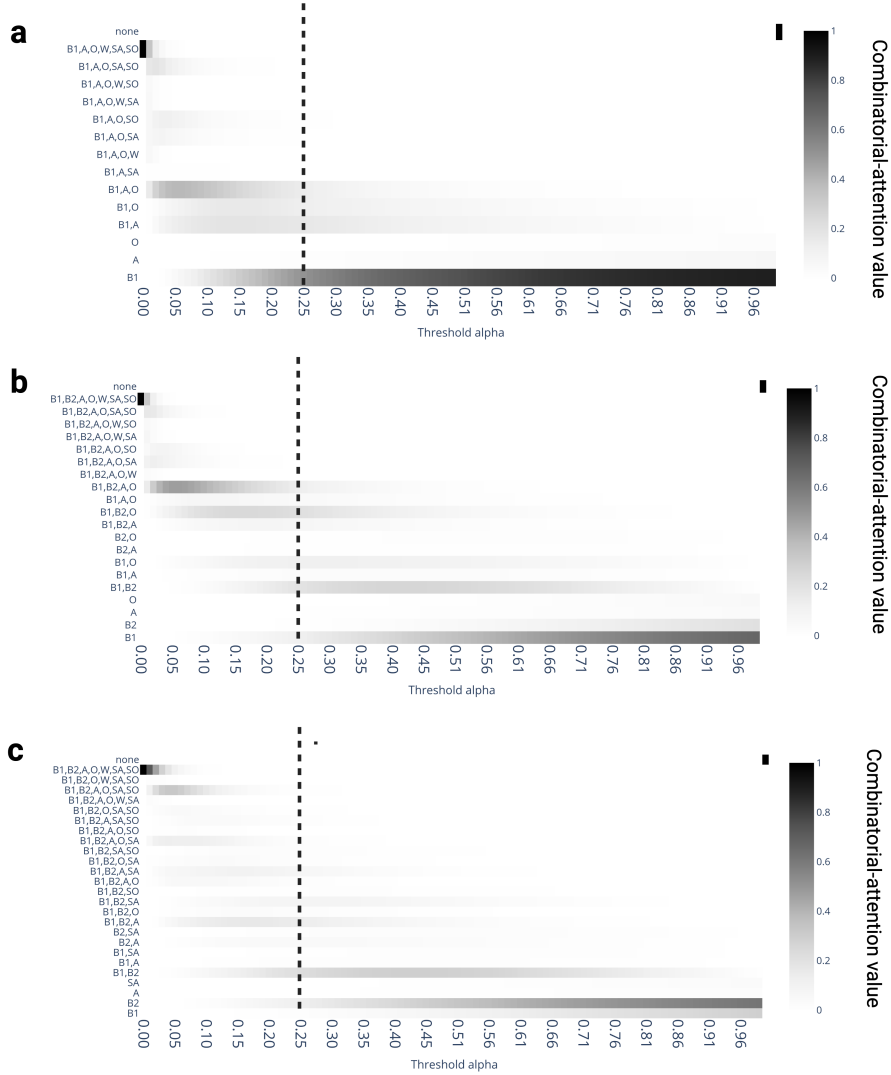


Figure 2: Combinatorial-attention values in function of alpha averaged over 20 trained agents for **a** version $v0$, **b** version $v1$ and **c** version $v2$. Dotted lines indicate $\alpha = 0.25$.

F Impact of the agent and opponent score displayed on the agents' behavior

Based on the observation that ATOMs exhibited a stronger focus on the scores of both the agents and their opponents in version $v2$ compared to versions $v1$ and $v0$, we investigated the potential impact of the displayed scores on the agent's decision to hit $B1$ or $B2$.

To examine this, we conducted the *Dual Ball Discrimination Test* across all combinations of displayed scores (ranging from 0 to 20 for the opponent and 0 to 40 for the agent) for each of the 50 agents trained on $v2$. In this test, the agent, given a specific score combination (score agent, score opponent), had to choose to hit $B1$ or $B2$ over 100 different trajectories. The set of 100 trajectories was consistent across all score combinations and agents.

This process generated two-dimensional matrices of dimensions 21×41 , where each matrix value represents the relative interaction of the agent with B1 , calculated as the ratio of the number of times the agent hit B1 to the total number of times the agent hit any ball. We standardized the relative interaction for each agent to account for variations in the average interactions of different agents. Using the standardized data, we computed a pairwise distance matrix with the 'correlation' metric and performed hierarchical clustering using the complete method. The resulting dendrogram is presented in Figure 3. Figure 4 illustrates the averaged heatmaps by clusters at a distance of 1.1, along with examples of heatmaps for models belonging to clusters three and five. Positive values (in red) indicate a preference for $B1$, while negative values (in blue) indicate a preference for $B2$. The findings reveal that the displayed scores influence the agent's choice to hit $B1$ or $B2$, with distinct patterns of influence emerging among different agents. For example, agents belonging to cluster five mostly interact with $B1$ until their displayed score get closer to 40 points where they tends to choose $B2$ over $B1$ (the game terminates when the agent reaches 41 points). Conversely, agents belonging to cluster three interact more with $B1$ or $B2$ in function of if the score of the opponent displayed is below or above 10 points.

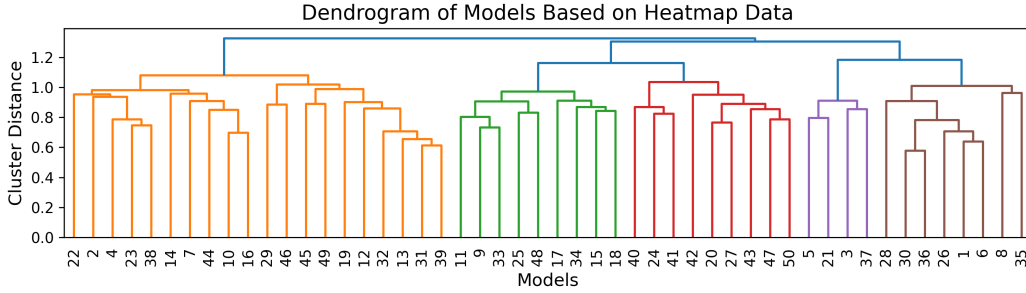


Figure 3: Dendrogram computed from the standardized interaction matrices of 50 agents trained on $V2$. Each interaction matrix is of size 21×41 corresponding to all combinations of score displayed.

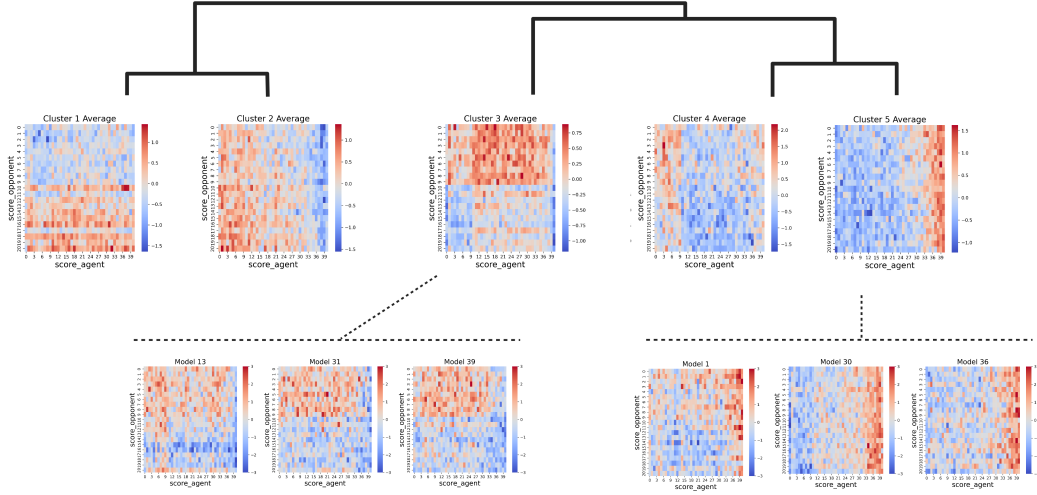


Figure 4: Dendrogram illustrating the hierarchical clustering of agents, with clusters identified up to a distance of 1.1, resulting in five main clusters. The heatmaps for each cluster were generated by averaging the heatmaps of all models within that cluster. The second row presents individual heatmaps from representative agents within clusters three and five.

G Color swap between B1 and B2

In this study, we investigated whether the color assigned to each ball affected the outcomes as measured by our metrics. We conducted this experiment by training 20 models for each game version, exchanging only the colors of balls B1 and B2. As observed on Figure 5, the color of the ball does not impact the hierarchical-attention pattern which is similar for both mapping of color to ball.

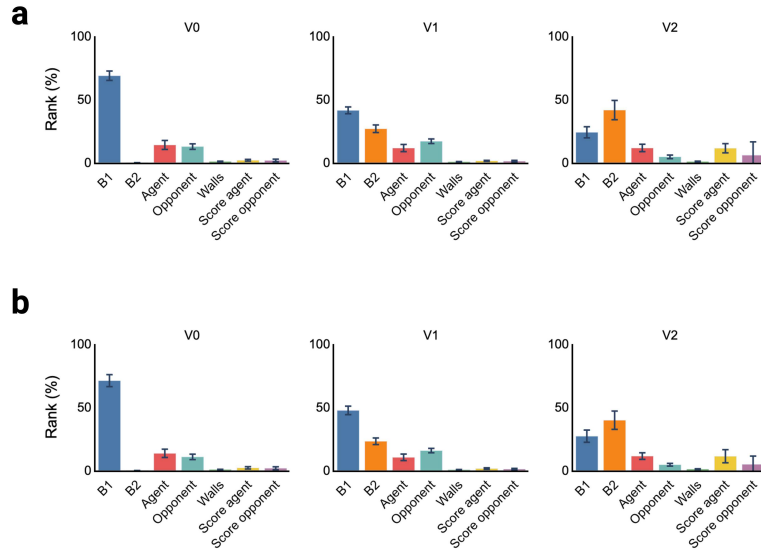


Figure 5: **a** Hierarchical attention average across 47 agents with an initial color mapping: B1 color (236, 236, 236) and B2 color (255, 255, 0). **b** Hierarchical attention average across 20 agents with a swapped color mapping: B1 color (255, 255, 0) and B2 color (236, 236, 236). Error bars represent the standard deviation.

H ATOMs for version v2 complete

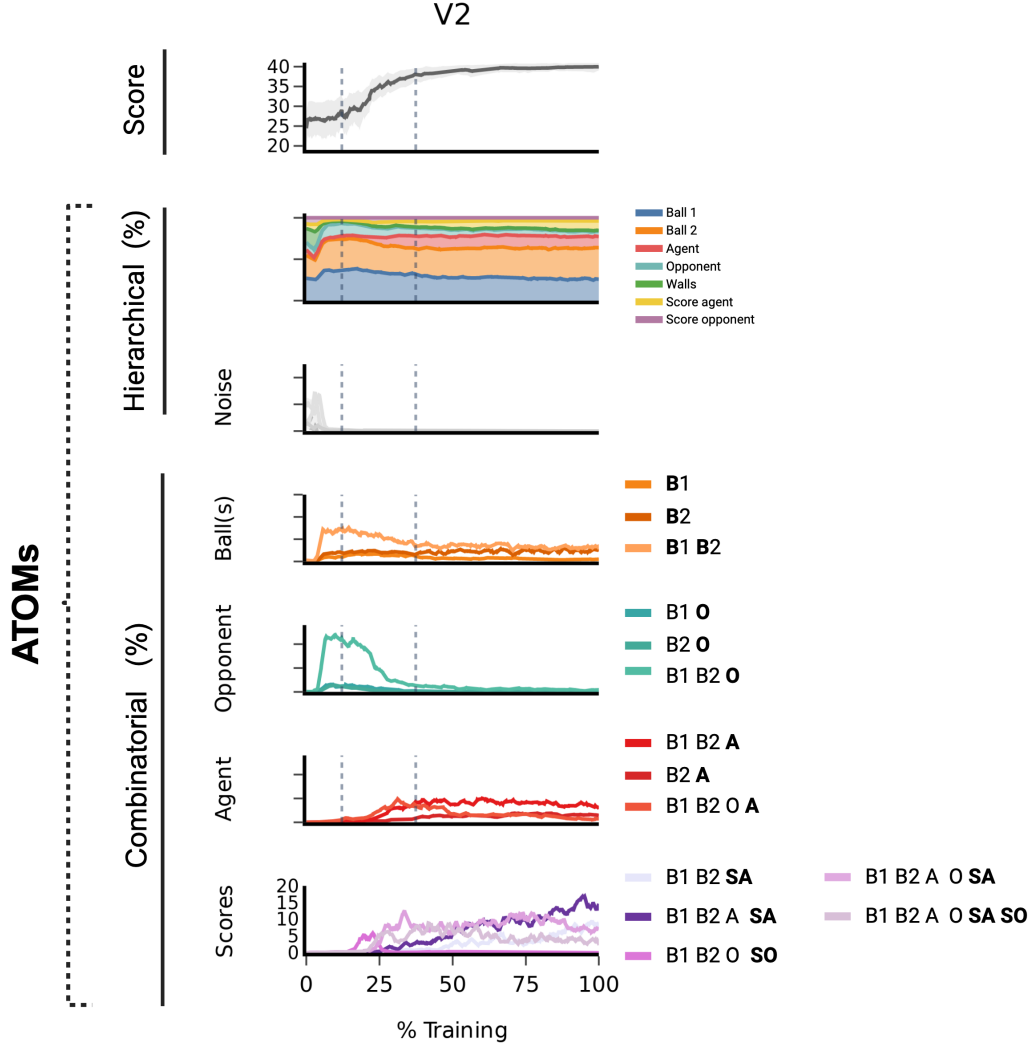


Figure 6: Development of the performance score and of ATOMs during learning for an agent trained on version v2. The performance scores of the agent is computed at each measurement over ten games. The dotted lines indicate the time frame during which the agent’s score showed a marked increase. These time frames were estimated manually. The average score is depicted by the central dark line, with the shaded region representing the standard deviation. The combinatorial-attention is categorized as follows from top to bottom: noise (grey), combinations of balls only (orange), combinations of opponent and balls (cyan), combinations of objects including the agent itself (red), and combinations of objects including the score opponent (SO) and the score of the agent (SA) (purple).

References

- Sebastian Bach, Alexander Binder, Grégoire Montavon, Frederick Klauschen, Klaus-Robert Müller, and Wojciech Samek. On pixel-wise explanations for non-linear classifier decisions by layer-wise relevance propagation. *PloS one*, 10(7):e0130140, 2015.
- Sebastian Lapuschkin, Stephan Wäldchen, Alexander Binder, Grégoire Montavon, Wojciech Samek, and Klaus-Robert Müller. Unmasking clever hans predictors and assessing what machines really learn. *Nature communications*, 10(1):1096, 2019.
- Grégoire Montavon, Sebastian Lapuschkin, Alexander Binder, Wojciech Samek, and Klaus-Robert Müller. Explaining nonlinear classification decisions with deep taylor decomposition. *Pattern recognition*, 65:211–222, 2017.
- Kai Fischer. Layer-wise relevance propagation for pytorch. <https://github.com/kaifishr/PyTorchRelevancePropagation>, 2021.
- Pete Shinnars. *PyGame*, 2011.
- Antonin Raffin, Ashley Hill, Adam Gleave, Anssi Kanervisto, Maximilian Ernestus, and Noah Dormann. Stable-baselines3: Reliable reinforcement learning implementations. *Journal of Machine Learning Research*, 22(268):1–8, 2021. URL <http://jmlr.org/papers/v22/20-1364.html>.
- Volodymyr Mnih, Koray Kavukcuoglu, David Silver, Alex Graves, Ioannis Antonoglou, Daan Wierstra, and Martin Riedmiller. Playing atari with deep reinforcement learning. *arXiv preprint arXiv:1312.5602*, 2013.